REVIEWS

Journal of Semiconductors
(2022) 43, 041104
doi: 10.1088/1674-4926/43/4/041104

In-situ monitoring of dynamic behavior of catalyst materials and reaction intermediates in semiconductor catalytic processes

Zhen Fang[1, 2, ‡], Yao Liu[3, ‡], Chengyi Song[1, 2], Peng Tao[1, 2], Wen Shang[1, 2], Tao Deng[1, 2], Xiaoqin Zeng[3, †], and Jianbo Wu[1, 2, 4, 5, †]

[1]State Key Laboratory of Metal Matrix Composites, School of Materials Science and Engineering, Shanghai Jiao Tong University, Shanghai 200240, China

[2]Center of Hydrogen Science, Shanghai Jiao Tong University, Shanghai 200240, China

[3]National Engineering Research Center of Light Alloy Net Forming, Shanghai Jiao Tong University, Shanghai 200240, China

[4]Materials Genome Initiative Center, Shanghai Jiao Tong University, Shanghai 200240, China

[5]Future Material Innovation Center, Zhangjiang Institute for Advanced Study, Shanghai Jiao Tong University, Shanghai 200240, China

Abstract: Semiconductor photocatalysis, as a key part of solar energy utilization, has far-reaching implications for industrial, agricultural, and commercial development. Lack of understanding of the catalyst evolution and the reaction mechanism is a critical obstacle for designing efficient and stable photocatalysts. This review summarizes the recent progress of *in-situ* exploring the dynamic behavior of catalyst materials and reaction intermediates. Semiconductor photocatalytic processes and two major classes of *in-situ* techniques that include microscopic imaging and spectroscopic characterization are presented. Finally, problems and challenges in *in-situ* characterization are proposed, geared toward developing more advanced *in-situ* techniques and monitoring more accurate and realistic reaction processes, to guide designing advanced photocatalysts.

Key words: *in-situ*; semiconductor photocatalyst; materials evolution; reaction intermediate

Citation: Z Fang, Y Liu, C Y Song, P Tao, W Shang, T Deng, X Q Zeng, and J B Wu, *In-situ* monitoring of dynamic behavior of catalyst materials and reaction intermediates in semiconductor catalytic processes[J]. *J. Semicond.*, 2022, 43(4), 041104. https://doi.org/10.1088/1674-4926/43/4/041104

1. Introduction

With the climate issues caused by the rapid development of industry and the energy demand brought by the increase in population, people face the problems of energy shortage and global warming. The development of semiconductor photocatalysts has realized these important reaction processes[1–3], including hydrogen evolution reaction, oxygen evolution reaction, CO_2 conversion, and N_2 fixation, which rely on abundant solar resources. It is of great significance for producing and collecting green hydrogen energy, the production of high value-added chemicals, batteries, nitrogen fertilizer, pollutant treatment, and other commercial and agricultural fields.

At present, semiconductor catalysts have received extensive attention and rapid development because of their green and pollution-free catalytic process and the effective catalytic ability for slow and complex kinetic processes. Nevertheless, there are still some obstacles. For example, photogenerated carriers are difficult to excite, have a high recombination rate and low transfer efficiency, and have low reaction activity on the catalytic surface. To solve these problems, researchers have proposed strategies such as heterojunction engineering[4–7], defect engineering[8], morphology regulation[9–11], element doping[12], and cocatalyst loading[9, 13] to design efficient, low-cost and large-scale semiconductor photocatalysts.

However, most of these studies focus on the changes of materials before and after the reaction, and the changes in the reaction process are not clear, which is of great significance to improve the stability of the catalyst. Therefore, it is necessary to further reveal the dynamic changes of materials and the changes of reaction intermediates at the surface and interface using *in-situ* or *operando* characterization methods and equipment, including microscopic imaging and spectral characterization (Fig. 1).

2. Semiconducting photocatalysis and *in-situ* characterization techniques

2.1. Principle of photocatalysis

The semiconductor is a kind of material with a unique energy band structure whose conductivity is between the conductor and insulator at room temperature. The special energy band structure of semiconductors consists of the valence band, conduction band, bandgap, and Fermi level (Fig. 2)[14]. Based on the presence or absence of impurities, semiconductors can be divided into intrinsic type, negative-type, and positive-type, respectively (Figs. 2(a)–2(c)). Generally, the energy band structure and electron distribution are different in different types of semiconductors.

A classical semiconductor photocatalytic process will undergo three critical processes (Fig. 2(d)): first, light absorp-

Zhen Fang and Yao Liu contributed to the work equally and should be regarded as co-first authors.

Correspondence to: X Q Zeng, xqzeng@sjtu.edu.cn; J B Wu, jianbowu@sjtu.edu.cn

Received 2 DECEMBER 2021; Revised 12 JANUARY 2022.

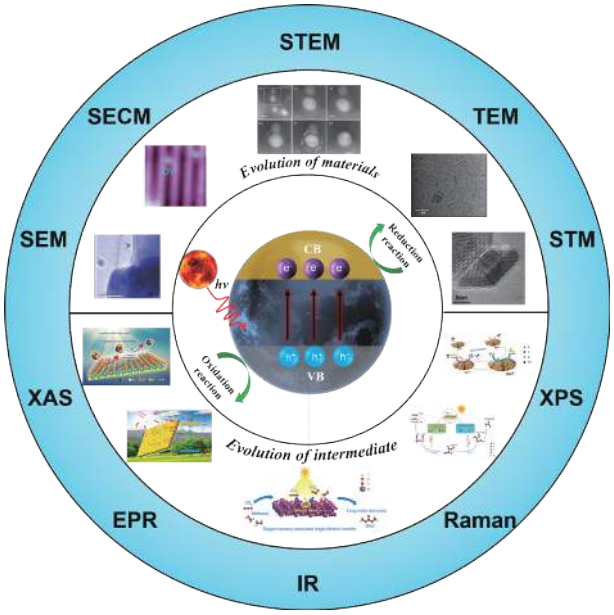

Fig. 1. (Color online) *In-situ* characterization of semiconducting photocatalysts for material research and mechanism disclosure in solar energy conversion and the storage process.

tion excites electron–hole pairs; second, the separation of photogenerated electron holes and transfer to the surface and interface of catalyst; third, the occurrence of reduction or oxidation half-reaction at the surface and interface of catalyst. In the photocatalytic process, some critical aspects need to be paid attention to. First, the semiconductor catalysts need to have a suitable energy band structure, including bandgap and energy level. A suitable energy gap can combine high carrier separation efficiency with excellent photocatalytic activity. Semiconductors with energy levels higher than redox potential are more conducive to photocatalytic reaction specifically, the low solar absorption caused by the wide bandgap is not favorable for separating electron–hole pairs. However, the narrow bandgap will produce electrons or holes with low reduction or oxidation potential, resulting in low photocatalytic activity. Therefore, bandgap and activity are two seemingly contradictory. Second, semiconductor catalysts need to have effective separation of photogenerated carriers and efficient surface transport to improve the activity and speed of photocatalytic reaction. Third, the catalysts need to have a relatively stable thermodynamic phase to improve the stability in the reaction processes[15], but this seems to be contrary to the high surface reaction activity. At present, semiconductor heterojunction engineering and defect engineering are considered to be effective measures to solve the existing problems.

In the process of the photocatalytic reaction, the catalyst material evolution will occur, such as atom migration and *in-situ* shelling, and a series of reaction intermediates will appear at the surface and interface of the catalyst. These evolutions have an important impact on the activity and stability of the catalytic reaction and the elaboration of the deeper reaction mechanism. Therefore, it needs to be characterized by matching *in-situ* techniques[15].

2.2. Characterization techniques to support and demonstrate

Modern advanced characterization techniques have been applied in the study of catalysts[16]. As shown in Fig. 3, when high-energy stimuli meet materials, materials will feedback various signals, and specific signal collectors can be used to obtain relevant material structure information. Photon rays and electron beams are the most common stimulus. After stimulating, the feedback signals include photon or electron diffraction signal, photon attenuation signal, electron energy signal, and so on. There are varieties of devices for collecting information, generally can be divided into two common technologies. One is spectroscopic technology, in which the change of physical properties and chemical composition of materials can be studied according to the spectroscopic signal absorbed or emitted by the material[17]. The other is microscopic imaging technology, which provides visible images of morphology and structure[18]. The principle of several advanced characterization methods in photocatalysts is introduced below in combination with Fig. 3 and helps us understand the applications.

X-ray photoelectron spectroscopy (XPS) is a comparatively surface-sensitive (about 10 nm depth) technology[19]. The principle of XPS is using X-rays to irradiate samples and result in the photoelectric effect (Fig. 3). Inner electrons or valence electrons of atoms or molecules are excited by photons and are named photoelectrons. The binding energy of photoelectrons can be measured and is specific to elements. Defects in catalysts can alter the electrical structure and chemical environment of the elements, resulting in spectrum variations such as peak shift, intensity fluctuation, or the formation of additional peaks[20]. In addition, changes in element-binding energy can accurately represent changes in electron density. As a result, binding energy changes can be utilized to analyze the direction of charge carrier transfer in heterojunction photocatalysts[21].

X-ray absorption spectroscopy (XAS) characterizes the material by measuring the absorption coefficient of X-ray[22]. The intensity of an X-ray is attenuated when it travels through a substance. If the incident X-ray energy is too low, the orbital electrons in the element are not excited. When the energy of the X-rays is strong enough to excite core electrons to the unoccupied state, the X-ray is significantly absorbed, resulting in a dramatic jump in the spectrum known as the X-ray absorption near edge structure (XANES). This part can be used to identify particular elements and is sensitive to the oxidization state. The core electrons stimulated to a continuous state create outgoing and scattering wave interference with nearby atoms as X-ray energy rises. Extended X-ray absorption fine structure (EXAFS) formed in this region reflects local atomic structures including bond distance and coordination number.

Infrared (IR) spectroscopies use infrared light to stimulate materials and probes dipole moment changes by the vibrations and rotations of bonds in molecules, functional groups, and radicals[23]. Although IR is not surface sensitive, it can discern the difference between free molecules and adsorbates bonded to solid surfaces in any environment due to small changes in vibrational frequencies.

Raman spectroscopy is another useful vibrational spectroscopy. This technique utilizes a visible light laser for excitation and measures the energy losses between incident photons and inelastically scattered photons, acquiring polariz-

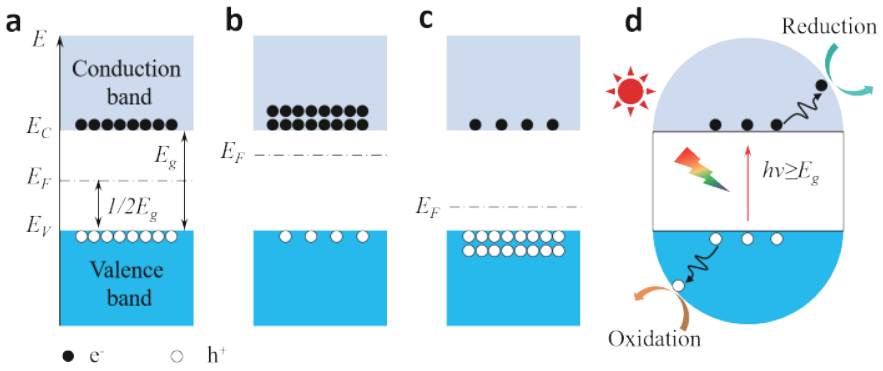

Fig. 2. (Color online) Energy band diagram and electron distribution of three typical types of semiconductors, including (a) intrinsic type, (b) negative-type, and (c) positive-type. (d) Mechanism displays of semiconductor photocatalysis.

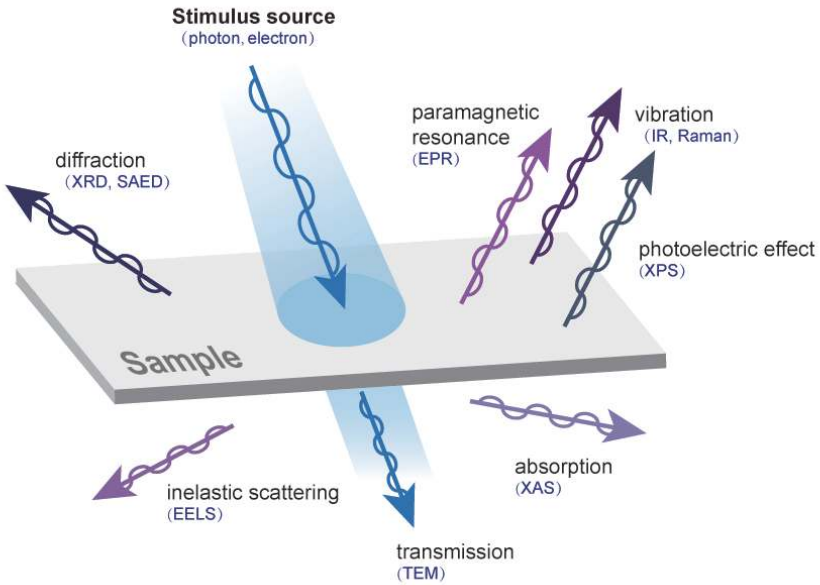

Fig. 3. (Color online) Schematic diagram of the interaction between particles (electrons and photons) and materials.

ability change in a sample under vibrational modes. Raman is very adept at identifying low-frequency modes, which are difficult to detect by traditional methods[24]. Sometimes Raman spectroscopy and IR spectroscopy can complement each other. Normal Raman signals are not enough inaccurate tracking of reaction, but surface-enhanced Raman spectroscopy (SERS) can help to solve it and show great potential in *in-situ* catalytic studies[25].

Electron paramagnetic resonance spectroscopy (EPR), also known as electron spin resonance (ESR), is a magnetic resonance technology to directly detect and study unpaired electron paramagnetic[26]. It is often used to detect single-electron capture vacancy defects in materials with high sensitivity. For example, if a material contains unpaired electrons, it will be subjected to an applied magnetic field. When this magnetic field is applied, the unpaired electrons in the material will align in a certain orientation, and Zeeman splitting will occur. The strength of the magnetic field is proportional. If electromagnetic waves with the same energy difference as the Zeeman split level are added to the vertical magnetic field direction, resonance occurs. The information of defect type and relative concentration was obtained according to *G* value and signal strength.

A transmission electron microscope (TEM) is commonly employed for direct observation of nanomaterials[27]. A high-energy electron beam is incident into a quite thin TEM sample, and the electrons elastic collide with the atoms in the material and change direction. The scattering angle is related to the sample's density and thickness, allowing the formation of various bright and dark pictures that will be magnified and focused on the imaging equipment. When equipped with a spherical aberration corrector, atomic resolution images can be achieved. Electron energy loss spectrum (EELS) and electron diffraction are auxiliary functions of the electron microscope and provide some extra information about material composition and structure[28]. EELS characterize the elemental composition, chemical bonding, and electronic structure of materials by detecting energy loss of incident electrons, which is caused by an inelastic collision between transmission electron and sample electron. In addition, when satisfying Bragg's equation, elastic electrons can form a diffraction pattern on the dorsal focal plane in diffraction mode and provide crystal structure information of materials. Selected-area electron diffraction (SAED) can analyze some specific microregions with an objective aperture. Scanning transmission electron microscopy (STEM) is another important imaging tech-

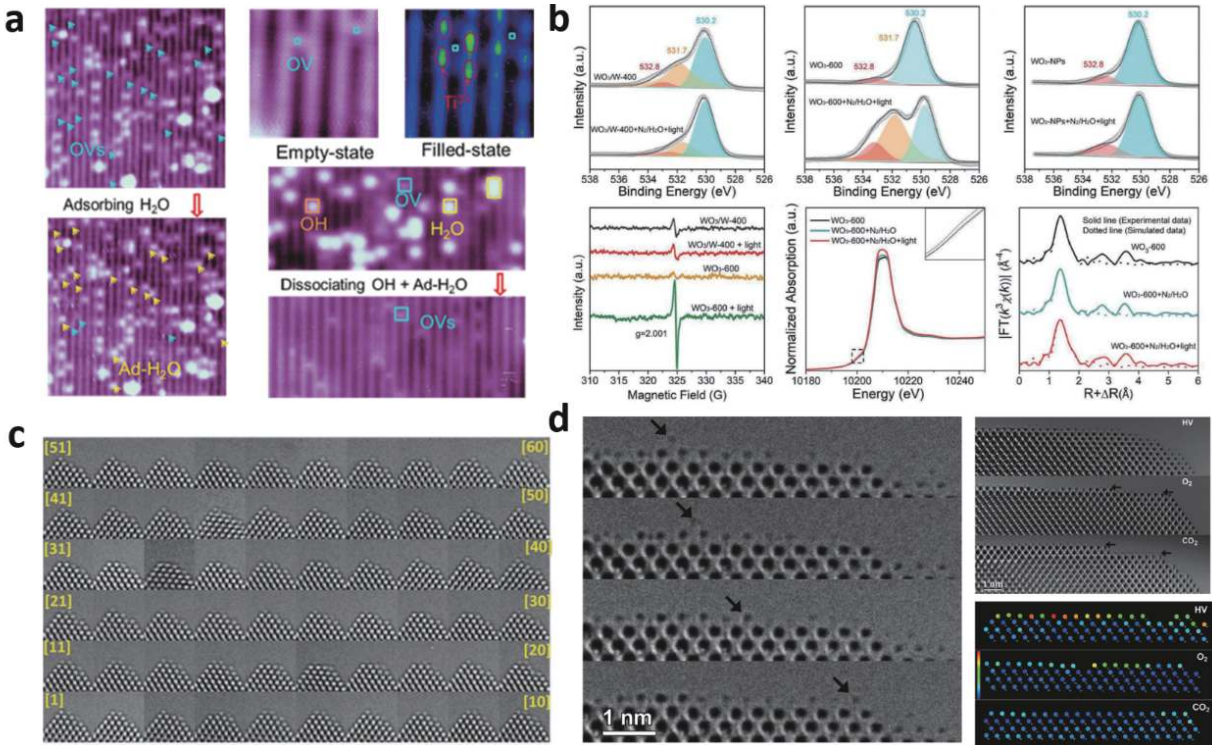

Fig. 4. (Color online) (a) *In-situ* STM observation of oxygen vacancies dynamic changes on TiO_2(110) surface. (b) *In-situ* XPS, *in-situ* EPR, *in-situ* XAS (XANES) and *in-situ* EXAFS spectra in R space of WO_3-600. (c) Series of *in-situ* TEM images of a CeO_2 nanoparticle. (d) *In-situ* TEM images of atom mobility on CeO_2 surface at {100} facet in high vacuum, oxygen, and carbon dioxide atmospheres. Modified with permission from (a) Ref. [32] Copyright 2018 American Chemical Society, (b) Ref. [33] Copyright 2019 WILEY-VCH Verlag GmbH & Co. KGaA, (c) Ref. [35] Copyright 2017 American Chemical Society, (d) Ref. [36] Copyright 2011 WILEY-VCH Verlag GmbH & Co. KGaA.

nology of electron microscope and is a clever combination of SEM and TEM. It uses a high-energy electron beam to scan thin samples, and the annular detector collects the high angle scattered electrons to image. STEM resolution has reached atomic scale, and *Z* contrast (where *Z* represents the atomic number of the atom) imaging can be obtained in STEM mode. In addition, the development of a dedicated environmental transmission electron microscope (ETEM) plus the modified TEM sample holders, which allow for the presence of either gas or liquid and make *in-situ* studies in TEM possible. *In-situ* TEM or STEM characterization of the photocatalytic process can be carried out after the introduction of light irradiation.

A scanning tunneling microscope (STM) uses the quantum tunnel effect to identify the atomic arrangement on the material's surface by measuring the tunneling current between the probe tip and the material surface[29]. After processing the tunnel current, the intuitive 3D surface image can be obtained. STM serves the following functions: identification of the surface structure, analysis of surface defects as well as investigation of adsorbate adsorption and dissociation behavior. Since the working environment of STM is not demanding, *in-situ* STM studies can monitor surface alteration of the photocatalyst during adsorption and reaction processes under liquid and atmosphere.

Scanning electrochemical microscopy (SECM) works on electrochemical principles and measures the electrochemical currents given by the oxidation or reduction of substances within a microzone, which is ideal for exploring the heterogeneous catalysis process considering that it combines the spatial resolution of scanned probe microscopy with the *in-situ* manipulation of electrochemical techniques[30]. The approach scans and obtains the associated micro-area electrochemistry and related information using extremely small electrodes (probes) driven close to the sample, which can be a conductor, insulator, or semiconductor.

3. Evolution of catalytic materials

3.1. Single-component semiconductors

When a single-component semiconductor is employed as a photocatalytic model, all charge-kinetics processes stated above can occur on the same semiconductor catalyst. As a result, their photocatalytic active surface change is relatively simple, including some defect dynamics and surface structural evolution. This part mainly introduces some examples of using *in-situ* technologies to monitor the evolution in single-component semiconductor catalysts and aids in the insight into the mechanism.

Defects play a crucial role in photocatalytic reactions since they are highly connected with the surface-active site[8]. For example, one of the most typical defects in metal–oxide–semiconductors is oxygen vacancy. The introduction of oxygen vacancy makes the metal atoms of metal oxides present an unsaturated coordination state and provides an effective channel for the transfer of electrons from the semiconductor to the adsorbed gas molecules[31]. Oxygen vacancies were found to change dynamically during photocatalysis in many studies. Fig. 4(a) shows a work clarifying the catalytic kinetics of oxygen vacancy on TiO_2(110) surface by *in-situ*

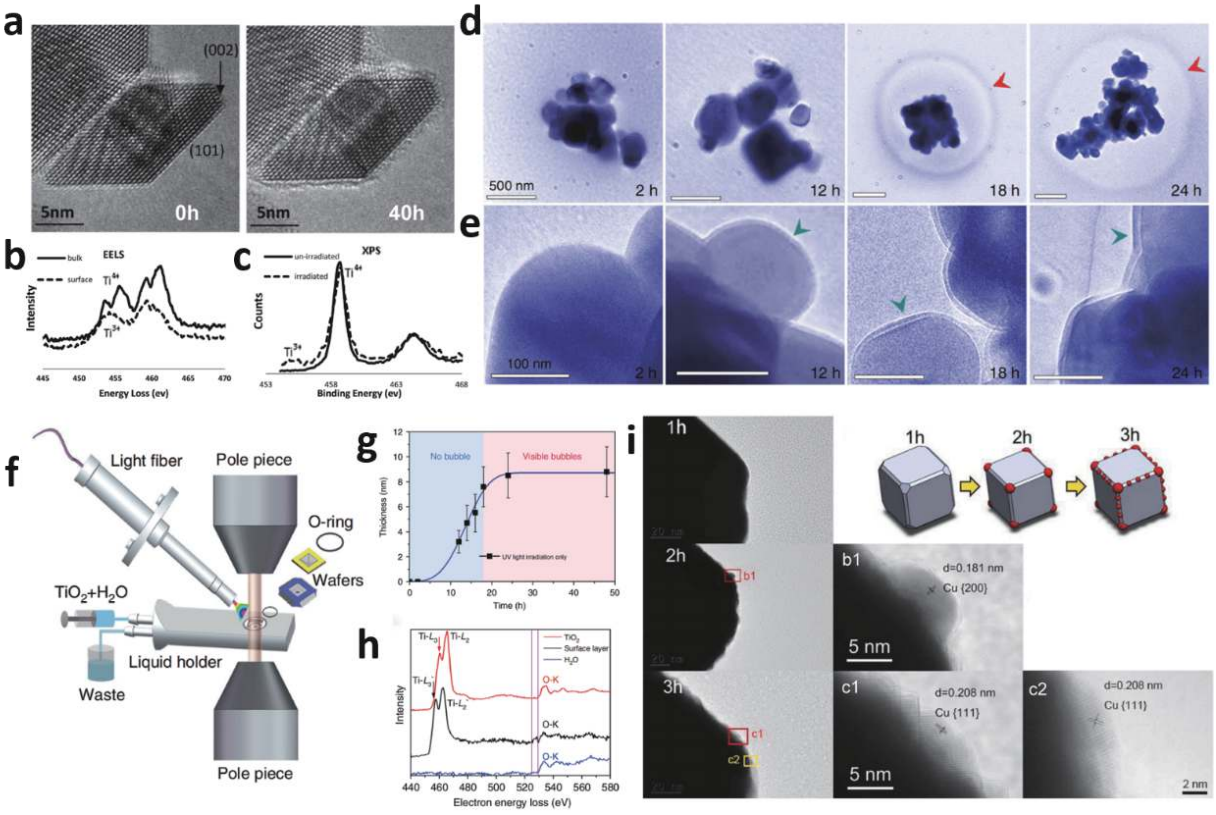

Fig. 5. (Color online) (a) *In-situ* TEM images of TiO_2 under water vapor conditions, with (b) EELS spectra and (c) XPS spectra of TiO_2 particles. *In-situ* TEM study of TiO_2 photocatalytic water splitting under UV light: (d) formation and evolution of bubbles, (e) magnified views of the surface shell on TiO_2, (f) schematic diagrams of fluidic TEM holder with *in-situ* UV illumination, (g) surface shell thickness on TiO_2 under UV illumination and (h) EELS spectra of the TiO_2. (i) HRTEM images of Cu_2O samples irradiated for 1, 2, and 3 h, as well as schematic diagrams of Cu_2O structure change during irradiation. Modified with permission from (a), (b) and (c) Ref. [38] Copyright 2013 American Chemical Society, (d), (e), (f), (g) and (h) Ref. [39] Copyright 2018 Springer Nature, (i) Ref. [40] Copyright 2020 Elsevier Ltd.

STM[32]. In this study, oxygen vacancies are the major structural defects on the surface of the TiO_2(110) single crystal. Before reaction, the adsorbed H_2O molecules are located at the oxygen vacancy site; with the catalytic reaction, the surface oxygen vacancy is repaired, while the second layer oxygen vacancy can exist stably. It indicates that some catalytic reactions take place at the cost of oxygen vacancy consumption. Besides, other experiments have found that *operando* oxygen vacancies can also be created in the catalytic process[33]. The defect evolution was monitored in real-time using *in-situ* XPS, ESR, and XAS during the N_2 reduction process (Fig. 4(b)). Quasi *in-situ* XPS was performed before and after treating a flowing H_2O vapor of N_2 with light for 30 min. Before the reaction, there was no indication of *operando* oxygen vacancies in WO_3-600, but after exposure to N_2 and H_2O under light irradiation, there was a significant signal for *operando* oxygen vacancies emerging. The generation of *operando* oxygen vacancies in WO_3-600 under catalytic condition was further verified by *in-situ* ESR and XAS.

Surface atom migration on specific facets of semiconductors often occurs under photocatalytic reactions, which may influence their catalysis and stability. Some works report that the inelastic scattering of electron beam in electron microscopy can bring about an effect similar to that of UV light[34]. While electron beam irradiation would be absent as a stimulant in real-world circumstances, the paths of atomic surface rearrangements are likely to be similar. It is of indirect relevance to applications in photocatalysis. The Ce atom migration has been studied by using an *in-situ* aberration-corrected transmission electron microscopy (AC-TEM), and 60 TEM images of the {100} facet at the CeO_2 nanoparticle corner were shown in Fig. 4(c)[35]. Atomic hopping activities were discovered reversible. On this basis, the mobility of Ce atoms at {100} facet in different atmospheres was characterized by an *in-situ* ETEM (Fig. 4(d))[36]. When under a high vacuum, Ce atoms were observed to change rapidly from one frame to the next. Under O_2 ambient circumstances, the (001) surface is now ended by oxygen columns, which inhibit the mobility of the Ce atoms. Furthermore, when CO_2 is injected into the chamber, surface mobility is entirely stopped.

With the advancement of *in-situ* TEM, it is possible to directly observe the chemical change process of catalyst surface during light irradiation rather than electron beam irradiation mentioned above[37]. Then understand the change of surface structure and active site in the real photocatalytic process. In addition, EELS or XPS can be adopted to prove the chemical composition of the material at each stage of the photocatalytic process. Crozier *et al.* used the ETEM to study TiO_2 nanoparticle surfaces in a true photocatalytic reaction with high-intensity broadband light and water vapor conditions[38]. The surface of TiO_2 was smooth and well crystalline when light and water vapor were first introduced, but then the surface became coarse and covered by a disordered TiO_2 amorphous layer after 40 h of reaction (Fig. 5(a)). The amorph-

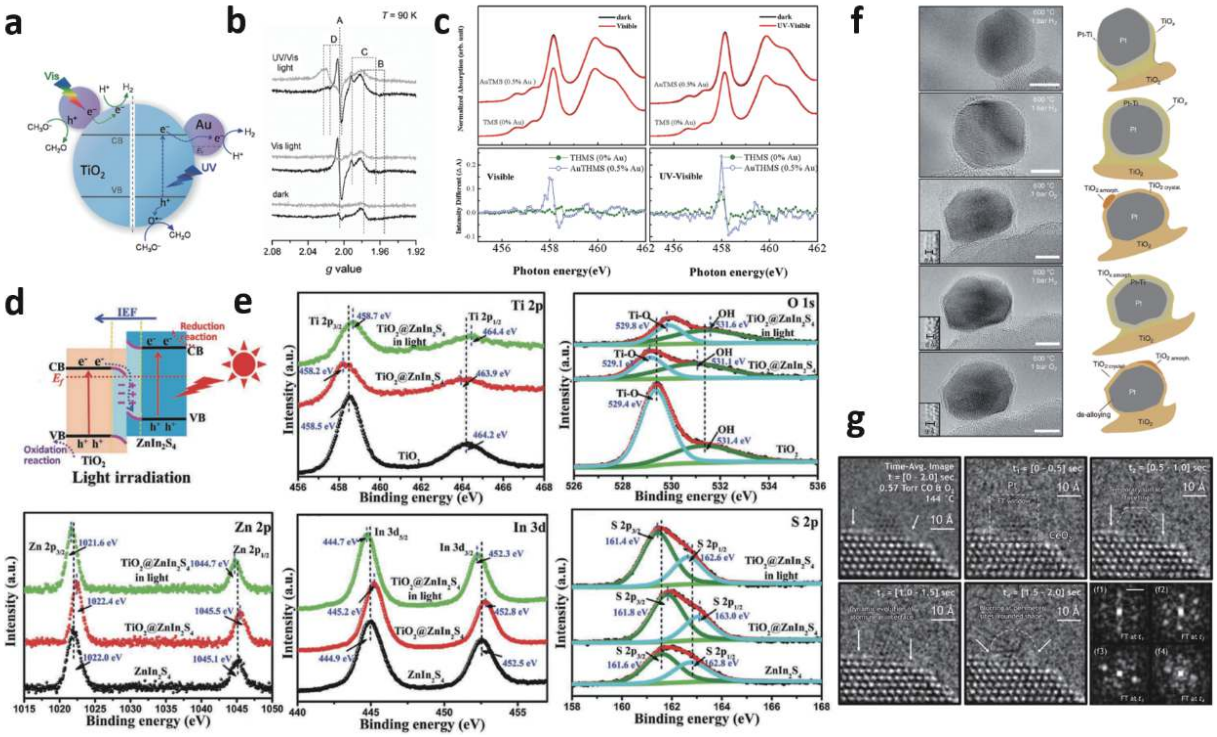

Fig. 6. (Color online) (a) Schematic diagram of water reduction in Au-TiO_2 with UV- (right) and visible-light (left) driven. (b) *In-situ* EPR spectra of TiO_2 and Au-TiO_2. (c) *In-situ* XAS spectra of THMSs and Au THMSs. (d) Schematic illustration of the electron transfer mechanism between TiO_2/Zn-In_2S_4 S-scheme heterojunction. (e) *In-situ* XPS spectra of TiO_2, $ZnIn_2S_4$, and TiO_2/$ZnIn_2S_4$. (f) *In-situ* TEM observations about evolution and dynamic structural changes of the overlayer in a strong metal-support interaction. (g) Time-series *in-situ* ETEM image of Pt-loaded CeO_2. Modified with permission from (a) and (b) Ref. [43] Copyright 2013 Wiley-VCH Verlag GmbH & Co. KGaA, (c) Ref. [44] Copyright 2018 American Chemical Society, (d) and (e) Ref. [52] Copyright 2021 Wiley-VCH GmbH, (f) Ref. [53] Copyright 2021 Springer Nature, (g) Ref. [54] Copyright 2020 Springer Nature.

ous layer showed very stable under further irradiation. The state of the Ti species was examined using EELS and XPS to determine the amorphous phase's composition (Figs. 5(b) and 5(c)), revealing that part of the surface layer was reduced to the Ti^{3+} state while the bulk stayed in the Ti^{4+}.

Since most characterizations for photocatalytic reactions of anatase TiO_2 are limited to water vapor environment, Sui *et al.* established a novel method to examine photocatalytic water splitting using anatase TiO_2 in a genuine reaction environment (Fig. 5(f))[39]. The photocatalytic reactions reported in water differ significantly from those observed in vapor. A shell layer formed on the surface of TiO_2 nanoparticles in the aqueous phase as the reaction proceeded, and bubbles formed around the TiO_2 nanoparticles subsequently (Figs. 5(d) and 5(e)). Fig. 5(d) shows the growth rate of the shell on TiO_2 and found it has a maximum thickness of around 8.8 nm. The components of the shells were studied with the use of EELS. In Fig. 5(h), the EELS data implies that Ti in the surface shell has a lower valence state. Authors proposed that hydrogen atoms will preferentially enter into the interior of TiO_2 lattice, leading to the transformation of Ti^{4+} to Ti^{3+} in the low state and then forming a nanoscale hydrogenation shell on the surface of TiO_2.

Yu *et al.* also obtained *in-situ* TEM observations of an unstable Cu_2O catalyst during a photocatalytic reaction. Fig. 5(i) shows HRTEM images of Cu_2O samples in continuous irradiation[40]. Within 1 h of light, the Cu_2O cubes had barely changed. After 2 h of exposure to light, the surface of Cu_2O became increasingly rough, and Cu particles initially formed in the corner. Cu on Cu_2O surface strewn from the corner to the edge of Cu_2O cubes when the illumination continued to 3 h. In this work, selected area electron diffraction (SAED) and other reduction experiments are used to further verify the generation of Cu. Finally, formed nano-Cu was verified to be the photocatalytic reaction's active site.

3.2. Multi-component semiconductor

To promote the photocatalytic efficiency of semiconductors, various studies forward from the single-component system to the multi-component hybrid system, like a metal–semiconductor hybrid, semiconductor–semiconductor hybrid, and so on[14]. Charge creation and consumption may occur simultaneously on separate components in multi-component semiconductors, and charge transfer is usually done from one component to another. Furthermore, additional interfaces between the various components can be active reaction sites and alter dynamically during reactions. In a word, with the improvement of catalyst performance, both charge kinetics and structure change become more complicated. This section will provide some applications of *in-situ* characterization of multi-component semiconductor photocatalysts.

Integration with metal can harness the charging kinetics of semiconductors. Especially some noble metals, such as Au, Ag, and Cu, which offer strong plasmonic properties, can improve the activity of semiconductors[41]. For example, TiO_2 has a wide bandgap and can only convert UV light into chemical energy. Au-loaded TiO_2 not only shows an improved activ-

ity in UV light than pristine TiO_2. And Au-loaded also brings an imparting strong visible-light photo absorption capability to TiO_2 (Fig. 6(a))[42]. The application of *in-situ* spectroscopy can provide a piece of reliable evidence on charge transfer mechanisms between metal and semiconductor under reaction conditions. Priebe *et al.* use an *in-situ* EPR to monitor water reduction over Au-TiO_2 catalysts. As shown in Fig. 6(b)[43], signal A is formed in Au-loaded TiO_2 irradiated with visible light. In contrast, no signal in pure TiO_2. Signal A reflects trapped electrons from Au nanoparticles, demonstrating that electrons driven by visible-light transfer from the Au to the TiO_2 surface, and are trapped by vacancies at the Au-TiO_2 interphase. Another work uses *in-situ* XAS to monitor Au-loaded TiO_2 hollow microspheres under visible-light illumination (Fig. 6(c)), also find the signal to prove that hot electron charge transfers due to surface plasmon resonance effect from Au 5d to Ti 3d t_{2g}[44].

Construction of heterojunctions in semiconductor–semiconductor photocatalysts is another way to steer the charging kinetics, such as extending the spectral range for light absorption and enhancing electron-hole separation[45, 46]. For instance, oxidation photocatalyst (OP) with low VB and low CB position displays strong oxidation ability but relatively low activity. Conversely, reduction photocatalysts (RP) stand out for their high CB position and large driving force for running the photocatalytic reduction reaction. Since various semiconductor materials have characteristic band structures, different combinations of semiconductor materials will form different junctions[4, 47–49]. The experimental requirement for demonstrating charge carrier transfer on heterojunction has always been a tough process[50, 51]. An *in-situ* XPS technique was used by Yu *et al.* to confirm a step-scheme (S-scheme) heterojunction mechanism on TiO_2/$ZnIn_2S_4$ for photocatalytic CO_2 reduction[52]. The schematic illustration and *in-situ* XPS are shown in Figs. 6(d) and 6(e). When TiO_2/$ZnIn_2S_4$ is in darkness, the binding energies of O 1s and Ti 2p shift to lower energy levels, and binding energies of Zn 2p, In 3d, and S 2p shift to higher energy levels, implying that the electrons transfer from $ZnIn_2S_4$ to TiO_2. After light irradiation, the binding energies shift reversely, suggesting the photo-generated electrons transfer from TiO_2 to $ZnIn_2S_4$ under light irradiation.

For multi-component semiconductors, the interfacial alterations of multiple components are also significant in the catalytic process. Many atomic-scale evolutions of the metal particle, oxide surface, and interface during catalysis remain unanswered. *In-situ* TEM is the best method to visualize atomic-scale dynamics. When there is a strong metal-support interaction (SMSI), metal nanoparticles can be reversibly covered when the support undergoes reduction. Bokhoven *et al.*, use an *in-situ* TEM to study an actual Pt/TiO_2 catalyst under changing gas atmosphere (Fig. 6(f))[53]. Pt develops a covering on its surface when exposed to hydrogen, and EELS mapping indicates that these species are Ti-containing. The overlayer abruptly increased after changing the gas environment to oxygen. When the gas environment was shifted back to hydrogen, dynamic changes occurred in the overlayer. And the overlayer decreased in thickness. As the interfacial energy undulates during the catalytic process, significant variation in metal particle form and bonding occurs, and the metal particle's adherence to the support may deteriorate. Crozier *et al.* employ *in-situ* AC-TEM to study the structural dynamics occurring at and near Pt/CeO_2 interfaces during carbon monoxide oxidation[54]. *In-situ* ETEM images and the Fourier transform (FT) are shown in Fig. 6(g). It can be found that diffuse intensity caused by fluxional dynamics appears at both the Pt nanoparticle and the perimeter of the Pt/CeO_2 interface.

4. Dynamic process of surface reaction intermediate

Accurate and intuitive observation of the dynamic process of reaction intermediates is helpful to reveal the mechanism of photocatalysis and design an advanced photocatalyst. *In-situ* monitoring provides an effective tool for detecting reaction intermediates in the whole photocatalytic process[55, 56]. The reaction intermediates and the intrinsic mechanisms involved in various catalytic processes are different, and herein some important single/multi-electron reaction processes are summarized.

4.1. Water photosplitting including HER and OER

The water-splitting, including hydrogen evolution reaction (HER) and oxygen evolution reaction (OER) (Fig. 7(a)), are key chemical reactions for green hydrogen production and energy conversion process[1, 2, 57]. The identification of reaction intermediates in the HER and OER processes is of significance for mechanistic understanding[58–63].

To monitor the water-splitting HER mechanism under realistic working conditions, Guo *et al.* proposed an *in-situ* measurement system combining linear-sweep voltammetry curves and *operando* Raman spectra and a possible HER mechanism of $MoS_{2x}Se_{2(1-x)}$ (Figs. 7(b)–7(d)). The spectra results show that H atoms are adsorbed to the active S/Se atoms (or atoms) to form intermediate MoS_2-H/$MoSe_2$-H and subsequent hydrogen desorption during the HER process[64].

In addition, *in-situ* diffuse reflectance infrared Fourier-transform (DRIFT) spectroscopy were performed to determine the possible reaction intermediates on the $ZnIn_2S_4$@MoS_2 in photocatalytic HER[65]. As shown in Fig. 7(e), a series of IR peaks at 3608, 1314, 1265, 1077, 1630, and 3440 cm^{-1} were monitored, in which 3608 cm^{-1} corresponds to the S–H, 1314 and 1265 and 1077 cm^{-1} correspond to the adsorbed O from SO_X, 1630 and 3440 cm^{-1} are assigned to the H_2O and OH, respectively. With the prolonged irradiation time in the presence of H_2O, the height of the peak at 3608 cm^{-1} gradually increased, meaning that the H atom tends to adsorb on S sites. Then the height of the peak at 3440 cm^{-1} is also raised after H adsorption reaches equilibrium. When turning on the Xe lamp, the intensity of peaks at 3608 and 3440 cm^{-1} gradually declined with the illumination time, verifying the activation of S–H and subsequent H_2 desorption process (Fig. 7(f)). Further, a possible reaction pathway for the HER process over the $ZnIn_2S_4$@MoS_2 with visible-light illumination was proposed in Fig. 7(g).

By analyzing the variations of infrared peaks after illumination with *in-situ* Fourier-transform infrared (FTIR) technique, Ye *et al.* studied the process of the HER on ReS_2/CdS under different sacrificial reagents, including Na_2S-Na_2SO_3 and lactic acid[66]. Specifically, for Na_2S-Na_2SO_3, the spectra result confirmed that H_2O will decompose and SO_3^{2-} will be oxidized to SO_4^{2-} (Fig. 7(h)). And according to the spectra result, lactic acid will decompose into -OH and -COOH, and then react with H_2O to form H_2 (Fig. 7(i)). Electron paramagnetic resonance (EPR) system was also used to detect the signal intens-

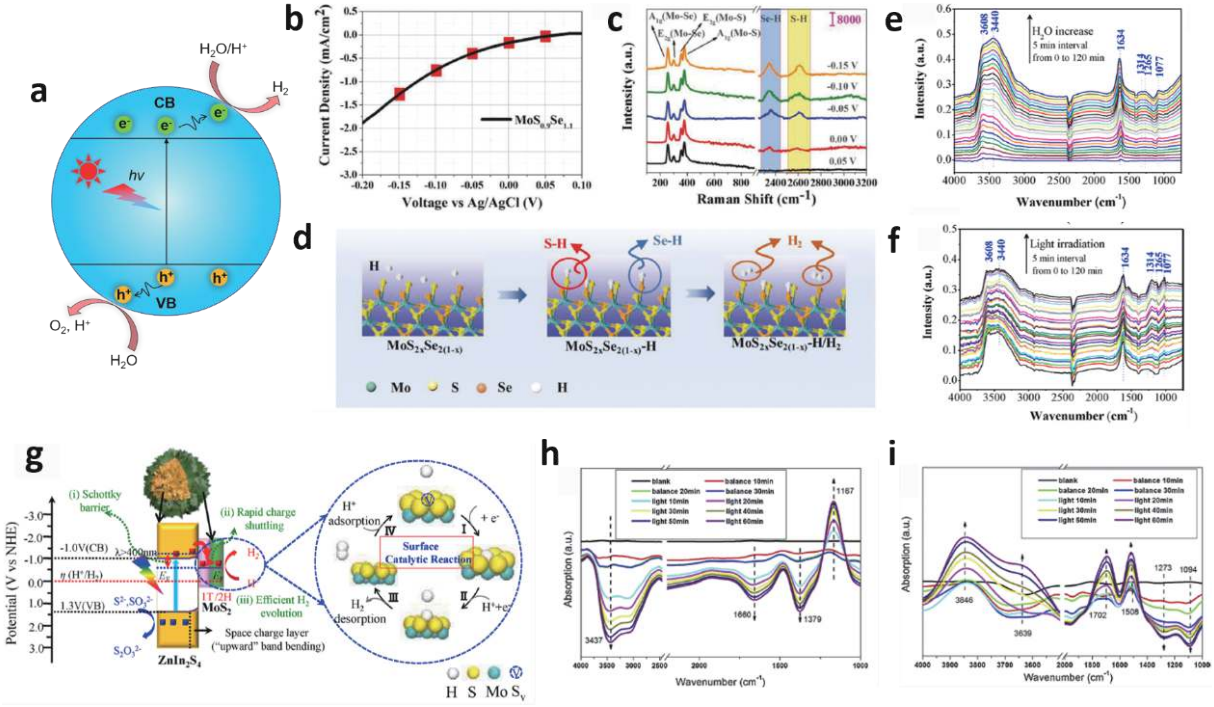

Fig. 7. (Color online) *In-situ* characterization of reaction intermediates in the photocatalytic HER and OER processes. (a) Mechanism scheme of HER and OER. (b) LSV curve (left) and (c) *operando* Raman spectra (right) of $MoS_{0.9}Se_{1.1}$. (d) Schematic illustration of the HER process in $MoS_{2x}Se_{2(1-x)}$. (e) *In-situ* DRIFT spectra of H_2O on the $ZnIn_2S_4$@MoS_2 with 2 h H_2O-saturated flow under He and (f) with a 2 h irradiation time under Xe lamp, and (g) proposed reaction pathway for the HER process over the $ZnIn_2S_4$@MoS_2. *In-situ* FTIR spectra of the HER process on ReS_2/CdS with two different sacrificial agents, (h) Na_2S-Na_2SO_3 and (i) lactic acid. Modified with permission from (b), (c) and (d) Ref. [64] Copyright 2020 Wiley-VCH Verlag GmbH & Co. KGaA, (e), (f) and (g) Ref. [65] Copyright 2021 Elsevier Ltd., (h) and (i) Ref. [66] Copyright 2019 Elsevier Ltd.

ity of $\cdot O_2^-$ to prove the direct Z-scheme charge migration mechanism in the S_v-ZIS/$MoSe_2$ system as an efficient HER photocatalyst[67].

Primary intermediates of ultraviolet light-induced OER on the TiO_2 (rutile) particles were monitored with *in-situ* MIRIR spectroscopy, and the results support the previously proposed OER mechanism[68]. By using time-resolved rapid-scan FTIR spectroscopy, two reaction intermediates of visible light-sensitized water oxidation on the Co_3O_4 were identified, and different catalytic sites were identified based on the kinetic behavior of the intermediates[69]. For $NaTaO_3$-based photocatalysts, according to the *in-situ* FTIR spectral results, the appearance of two new water oxidation intermediates, corresponding to the 1058 and 935 cm^{-1} peak positions, was thought to be derived from $Ta(_{VI})$=O and $Ta(O_2)$ peroxo species, respectively[70].

4.2. CO_2 conversion

Solar CO_2 conversion, including CO_2 photoreduction and CO_2 photofixation to valuable chemicals (Fig. 8(a)), play an important role in energy storage and global warming[71–76]. The evolution of intermediates and possible reaction mechanisms based on different CO_2 conversion reactions are summarized[77–79].

Based on defect engineering, Wu *et al.* designed a kind of BiOBr layers with enriching oxygen vacancies and adopted *in-situ* FTIR spectroscopy to monitor the reaction intermediates during CO_2 photoreduction to CO[80]. With the increase of radiation time, seven IR absorption peaks gradually appear (Fig. 8(b)). Among them, the two IR peaks at 1550 and 1200 cm^{-1} are derived from the COOH*, which verify that the COOH* are reaction intermediates. Further, a possible pathway for CO_2 photoreduction has been proposed (Fig. 8(c)): the CO_2 adsorption and H_2O dissociation occur simultaneously, and the adsorbed CO_2* interacts with the surface protons to produce COOH*, and further protonation of COOH* to generate the CO*.

Chen *et al.* explored that the important role of oxygen vacancy confined in Bi_2O_3 nanosheets in the conversion process of CO_2 and elaborated the reaction mechanism of CO_2 photofixation to long-chain chemicals by *in-situ* DRIFT spectroscopy[81]. As shown in Fig. 8(d), after irradiation of the OV-rich-Bi_2O_3 nanosheets in the presence of CO_2 and CH_3OH, three new IR peaks at 1294, 1456, and 1779 cm^{-1} appeared, corresponding to $\cdot CO_2^-$, CO_3= and dimethyl carbonate (DMC), respectively. With the increase of illumination time, it can be seen that the intensity of these peaks gradually increases and the $\cdot CO_2^-$ tends to stabilize. However, the product of DMC continues to rise. Based on the monitored intermediates, a reasonable reaction mechanism was proposed as schematically illustrated in Fig. 8(e).

With *in-situ* DRIFT spectroscopy, Wang *et al.* detected carbon-based species formed on the surface of S-scheme core-shell TiO_2@$ZnIn_2S_4$ heterojunction photocatalyst during photocatalytic CO_2 reduction reaction (Fig. 8(f))[52]. After light irradiation, several absorption peaks of key reaction intermediates are generated, including COO^-, $HCHO^-$, $HCOO^-$ and CH_3O^-, which show that the effective photoreduction process of CO_2 on the TiO_2@$ZnIn_2S_4$ and reveal a possible CO_2 conversion pathway (Fig. 8(g)).

The photothermal effect is not emphasized in traditional

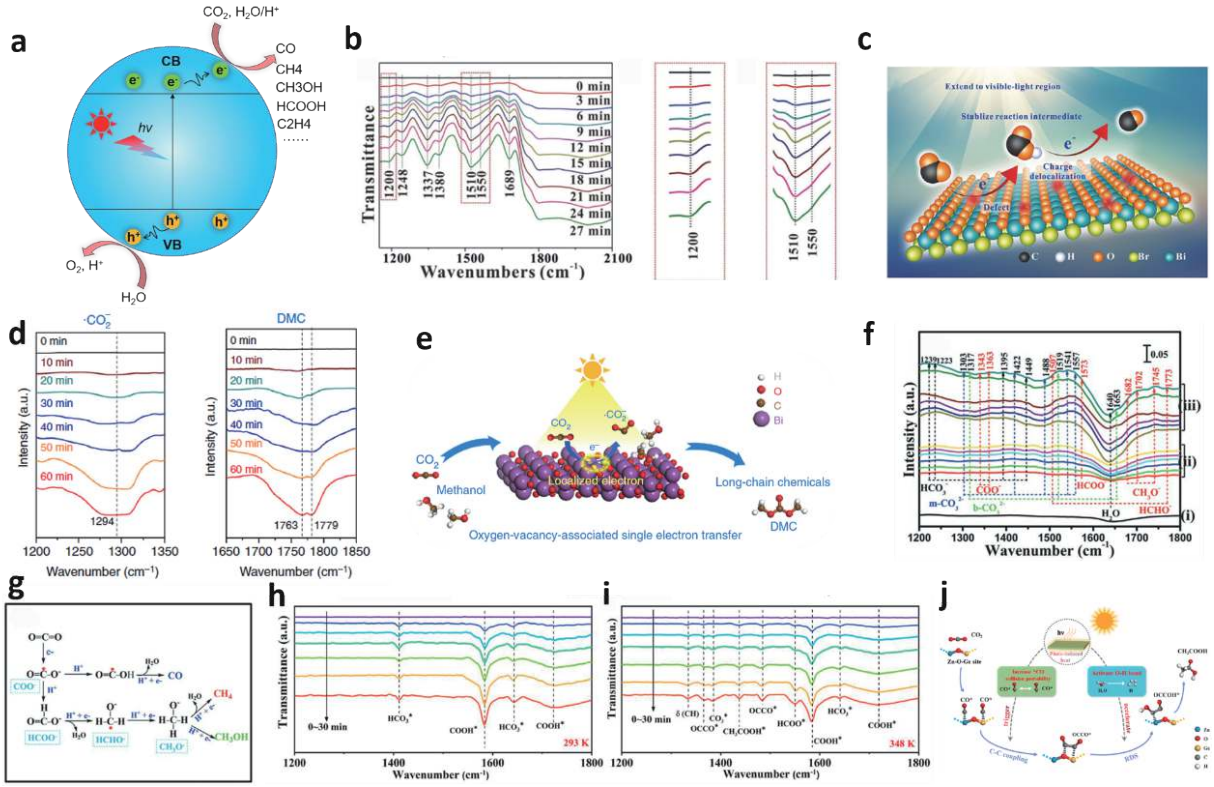

Fig. 8. (Color online) *In-situ* characterization of reaction intermediates in the photocatalytic CO_2 conversion processes. (a) Mechanism scheme of CO_2 conversion. (b) *In-situ* FTIR spectra of CO_2 adsorbed on the BiOBr layers with oxygen vacancy in the presence of H_2O vapor. (c) Schematic illustration for CO_2 photoconversion into CO over the oxygen-vacancy BiOBr. (d) *In-situ* DRIFTS spectra for the conversion process of CO_2 in the presence of CH_3OH under Xe lamp for oxygen vacancy-rich-Bi_2O_3 nanosheets. (e) Schematic illustration for CO_2 photofixation to long-chain chemicals. (f) *In-situ* DRIFTS spectra of CO_2 reduction reaction and (g) possible photocatalytic pathways over the TiO_2@$ZnIn_2S_4$. *In-situ* FTIR spectra of atmospheric 0.03 vol % CO_2/Ar photothermal reduction over the oxygen vacancy-rich Zn_2GeO_4 nanobelts at (h) 293 K and (i) 348 K. (j) Function mechanism of photoinduced heat during CO_2 photoreduction to CH_3COOH. Modified with permission from (b) and (c) Ref. [80] Copyright 2021 Wiley-VCH GmbH, (d) and (e) Ref. [81] Copyright 2019 Springer Nature, (f) and (g) Ref. [52] Copyright 2018 Wiley-VCH Verlag GmbH & Co. KGaA, (h), (i) and (j) Ref. [82] Copyright 2021 American Chemical Society.

photocatalytic systems. To reveal the CO_2 reduction intermediates and to further address the role of photothermal during the photocatalytic reactions, *in-situ* FTIR experiments were conducted at different temperatures with the oxygen vacancy-rich Zn_2GeO_4 nanobelts[82]. With the extending light irradiation time, the adsorbed CO_2 was converted into COOH* and CO* at 298 K (Fig. 8(h)), whereas the photothermal effect induced the coupling of CO* to form OCCO* at 348 K (Fig. 8(i)). Therefore, the C–C coupling step can be achieved by the photoinduced heat effect (Fig. 8(j)). In addition, *in-situ* FTIR spectral was used to prove that the COOH is the critical reaction intermediate in the process of CO_2 photoreduction to CO and CH_4 on the BiOX[83].

4.3. N_2 fixation

Ammonia, an important raw material for nitrogen fertilizer, is synthesized from N_2 and H_2 under high temperature and pressure using the Haber–Bosch process[84]. To address energy and environmental issue, a photocatalytic nitrogen fixation strategy with atmospheric pressure and ambient temperature was proposed (Fig. 9(a))[3, 85–87]. The evolution of intermediates and possible reaction mechanisms based on photocatalytic nitrogen fixation reactions are summarized[88–96].

Li *et al.* developed a simple low-temperature synthesis method to obtain a series of Bi_5O_7Br nanostructures[94]. The nitrogen photofixation reaction dynamics were detected by an *in-situ* IR system with a synchrotron radiation light source. *In-situ* IR spectra of Bi_5O_7Br-40 (40 °C of thermal treatment temperature) show that the intensity of several IR peaks changes with adsorption and irradiation time. Peak i to peak vi are assigned to N–H (3555 cm^{-1}), -OH (3360 cm^{-1}), NH_4^+ (2874 cm^{-1}), CO_2 (2359 cm^{-1}), N_2 (1624 cm^{-1}) and NH_3 (1557 cm^{-1}), respectively. (Fig. 9(b) and 9(d)). Upon visible light (Fig. 9(c)), the intensity of peaks i, iii, and iv decreases, while the intensity of peaks ii, v, and vi increases, which indicates the enhanced process of N_2 adsorption, activation, and N–H conversion to NH_3 (Fig. 9(c)). By comparing Fig. 9(a) and Fig. 9(d), the intensity of peaks i and iii increases, while the intensity of peak v decreases, indicating the effective breakage of the N≡N triple bond and the production of NH_4^+. By comparing Fig. 9(c) and Fig. 9(e), the intensities of peaks i and ii remain unchanged after turning off the light source while the intensities of peaks iii, iv, and vi increase, suggesting that an increase in N-H concentration and N_2 adsorption. These spectra results reveal that the preparative adsorption of N_2 on the Bi_5O_7Br-40 may be responsible for its outstanding N_2 photofixation performance.

Wang *et al.* utilized *in-situ* DRIFT spectroscopy to investigate the evolution of N-related intermediates in the early stages on the Bi_5O_7Br-NT[95]. With the increase of irradiation

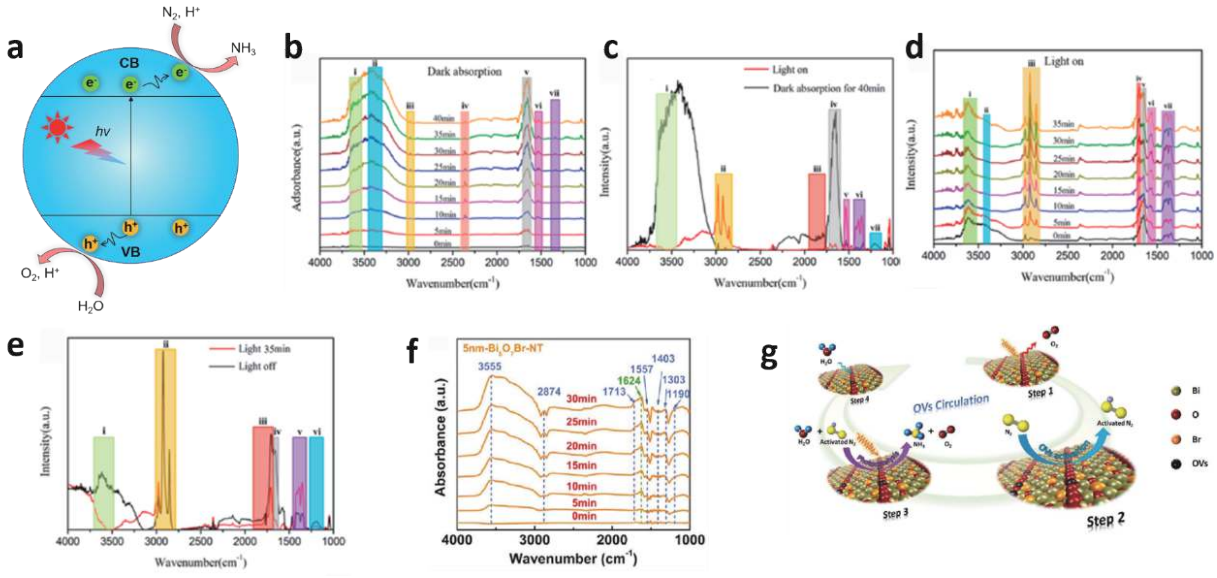

Fig. 9. (Color online) *In-situ* characterization of reaction intermediates in the N_2 photofixation process. (a) Mechanism scheme of N_2 fixation. *In-situ* IR spectra of Bi_5O_7Br-40 in the process of (b) N_2 adsorption from 0 to 40 min in the dark, (c) afterward receive visible light illumination, (d) then visible light illumination lasts 35 min, and (e) finally the visible light illumination is turned off. (f) *In-situ* DRFTIRS spectra were obtained and (g) a reaction pathway of N_2 photofixation over the Bi_5O_7Br nanotubes. Modified with permission from (b), (c), (d) and (e) Ref. [94] Copyright 2020 American Chemical Society, (f) and (g) Ref. [95] Copyright 2020 American Chemical Society.

time, several IR bands gradually increased (Fig. 9(f)), where 3555 & 1713 & 1667 cm^{-1}, 1403 & 2874 cm^{-1}, 1713 & 1557 cm^{-1}, and 1624 cm^{-1} are assigned to N–H, NH_4^+, NH_3 and N_2, respectively. The spectra show that the intensity of N≡N will continuously decrease in the form of OV–N≡N and N≡N will breakage to NH_3 or NH_4^+. Therefore, the N_2 photofixation mechanism over the Bi_5O_7Br-NT could be proposed as shown in Fig. 9(g).

To directly observe the mechanistic process of N_2 photoreduction, Li *et al.* used *in-situ* DRIFT spectroscopy to monitor the evolution channel of reaction intermediates on the BiOBr within a well-designed reaction cell[93]. As for BOB-001-OV with {001} facet-exposed, several IR signals gradually increased with the extension of irradiation time in the N_2 atmosphere, but no obvious signal appears on the BOB-001-H (reference photocatalyst without OVs). The spectra result verified that the significance of OVs on the N_2 photofixation on the BiOBr.

4.4. Other catalytic processes

In addition to the above catalytic process, some other critical reactions[97–100], such as NO removal, oxygen reduction reaction (ORR), are also proposed here.

NO from industrial emissions is considered an important contributor to air pollution and has adverse effects on human health[101]. The selective and effective removal of NO by a photocatalyst is an environment-friendly and cost-efficient way, compared with the traditional treatment method of high temperature and pressure[102, 103].

Shang *et al.* designed a kind of oxygen vacancy rich-blue TiO_2 photocatalyst for highly selective removal of NO and proved the reaction mechanism of selective NO removal[98]. As shown in Figs. 10(a) and 10(b), with the extension of lighting time, the increased absorption peaks of 1700–1100 cm^{-1} could be assigned to monodentate (1326 and 1282 cm^{-1}) and bidentate (1607, 1460, 1120, 1577, and 1469 cm^{-1}) nitrates over the TiO_2-OV and TiO_2. In contrast, increased new peaks at 1690 and 1142 cm^{-1} were confirmed for NO^+ and NO_2^- over the TiO_2 (Fig. 10(b)). The comparative spectra result between TiO_2-OV and TiO_2 prove that the photogenerated holes are the cause of NO_2 production. Thus, the mechanism of selective NO removal was demonstrated (Fig. 10(c)).

In addition, the *in-situ* FTIR spectra were used to analyze the time-dependent NO oxidation process in the presence of Bi^0OVs-$(BiO)_2CO_3$[97]. Several IR peaks representing nitrogen species appear with the extending irradiation time, which reveals the existence of multiple NO oxidation pathways (Fig. 10(d)). Therefore, the reaction mechanisms of three possible NO removal pathways over Bi^0OVs-$(BiO)_2CO_3$ were proposed (Fig. 10(e)).

Adsorbed hydroxyl radical $\cdot OH_{(ads)}$ is an important surface immediate for photocatalysis reaction of TiO_2[56]. Surface interrogation-scanning electrochemical microscopy (SI-SECM), a means of local monitoring of materials that combine high resolution and composition detection, is used for studying the dynamic behavior of $\cdot OH_{(ads)}$ on a TiO_2 substrate electrode with nano-size structure[100]. A typical SI-SECM operation mode is made up of three steps: pre-processing of the SI-SECM system under the dark condition and a negative feedback tip current will be observed for the first step; generation of $\cdot OH_{(ads)}$ under light irradiation and subsequently a time decay of $\cdot OH_{(ads)}$ in the dark and no tip current will be displayed for the second step; interrogation of $\cdot OH_{(ads)}$ in the dark and a transient positive feedback tip current will be observed for the final step. Surface intermediates of photocatalytic oxygen reduction reaction (ORR) on the TiO_2 films in aqueous solutions were directly detected with *in-situ* FTIR for the first time and a possible reaction mechanism was proposed[104].

5. Conclusion and prospects

Despite these advances in the field of *in-situ* characteriza-

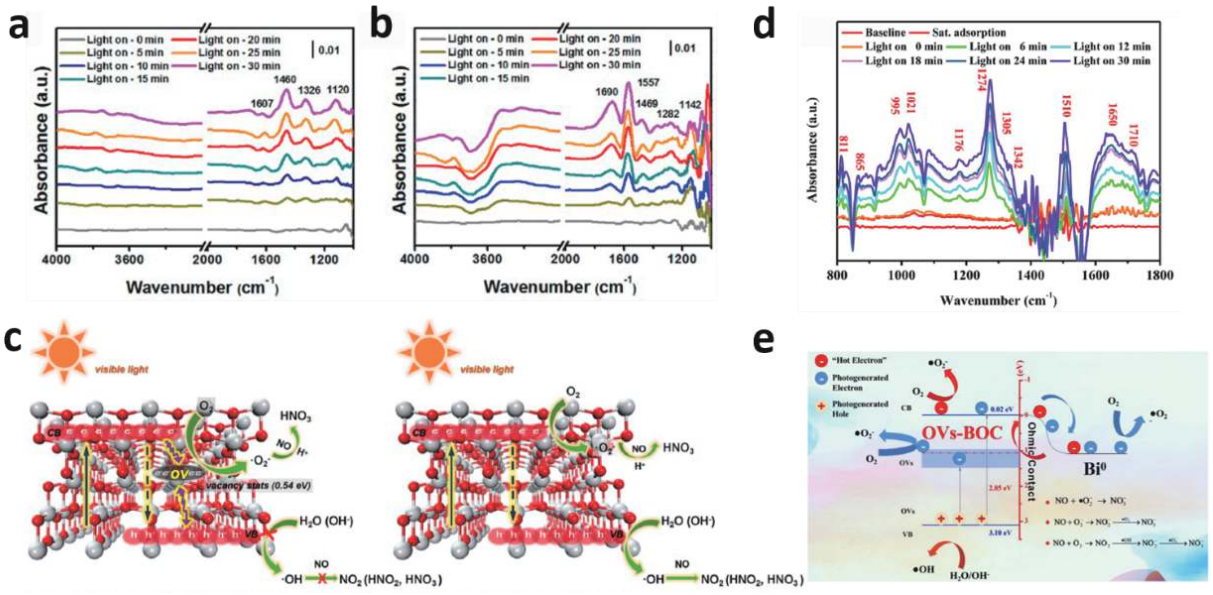

Fig. 10. (Color online) *In-situ* characterization of reaction intermediates in other catalytic processes. *In-situ* FTIR spectra of (a) TiO_2-OV and (b) TiO_2. (c) Selective removal mechanism during the NO removal process over the TiO_2-OV and TiO_2. (d) *In-situ* FTIR spectra and (e) NO removal mechanism of Bi_0OVs-$(BiO)_2CO_3$. Modified with permission from (a), (b) and (c) Ref. [98] Copyright 2019 American Chemical Society, (d) and (e) Ref. [97] Copyright 2019 Elsevier Ltd.

tion of photocatalysis, there is still an urgent need to further develop advanced and robust techniques to track the evolution of materials and reaction intermediates to gain a deeper understanding of the material changes and reaction mechanisms in the process of photocatalytic reactions.

For *in-situ* spectroscopic characterization, it is necessary to accurately control the reaction temperature, pressure, and atmosphere, and reduce the influence of the reaction device, so as to realize *in-situ* monitoring under real reaction conditions. Therefore, rational design of the *in-situ* device is required, for example, using more accurate probing thermocouples as close to the reaction system as possible without affecting the reaction environment. Use inert materials to design the reaction device to avoid the impact on the reaction environment at high temperatures. In addition, transient spectroscopy techniques with higher temporal resolution should be emphasized to monitor the kinetic behavior of active sites and reaction intermediates.

For microscopic imaging technology, especially *in-situ* TEM, the pursuit of high resolution (including spatial resolution and time resolution) is an eternal topic. Since catalysis reactions often occur at breakneck speed, time resolution needs to be improved with a good image signal-to-noise ratio to capture the dynamics and identify more intermediates in catalysis reactions. The advancement of electron detection can be quite beneficial. Like the newly developed approach allows for the detection of a single electron without the need to convert it to photons. The *in-situ* TEM can be utilized to examine dynamics on a millisecond time scale with this feature. The ultrafast TEM uses a brief electron pulse with a high current density and has a time resolution of up to femtoseconds. Ultrafast electron diffraction, in particular, can be used to investigate catalytic reactions with a significantly better temporal resolution.

Meanwhile, *in-situ* TEM needs to strike a balance between radiation damage and image resolution. Radiation damage is mainly caused by high-energy electron beams. When a sample is not resistant to radiation, the greatest defense is to lower the energy of the electron beams. The electron beam can be reduced while keeping acceptable resolution using spherical aberration-corrected electron microscopy. Note that when EDS and EELS are adopted, samples must be exposed to relatively high-energy electrons. It can be considered to carry out EDS and EELS analysis after the imaging characterization, which can reduce the generation of false images and improve the accuracy of experiments. In addition, updating the reaction cell materials to increase chip mechanical strength and chemical resistance would result in reduced window bulging, reducing the thickness of the liquid or gas layer, and so boosting spatial resolution.

Finally, the *in-situ* characterization process should organically combine a variety of *in-situ* techniques, including spectroscopy, microscopic imaging, and performance monitoring systems, to achieve a comprehensive and multidimensional information tracking of catalyst materials and reaction intermediates during the photocatalytic reaction. In addition, it is also necessary to focus on the whole photocatalytic process from beginning to end to elaborate on the real reaction mechanism and provide a deeper perspective on the design of advanced catalysts.

Acknowledgements

The work was supported by the National Science Foundation of China (21875137, 51521004, and 51420105009), Innovation Program of Shanghai Municipal Education Commission (Project No. 2019-01-07-00-02-E00069), the 111 Project (Project No. B16032), and the fund from Center of Hydrogen Science and Joint Research Center for Clean Energy Materials at Shanghai Jiao Tong University for financial supports.

References

[1] Maeda K, Teramura K, Lu D, et al. Photocatalyst releasing hydro-

gen from water. Nature, 2006, 440, 295
[2] Zhang Y C, Afzal N, Pan L, et al. Structure-activity relationship of defective metal-based photocatalysts for water splitting: Experimental and theoretical perspectives. Adv Sci, 2019, 6, 1900053
[3] Foster S L, Bakovic S I P, Duda R D, et al. Catalysts for nitrogen reduction to ammonia. Nat Catal, 2018, 1, 490
[4] Xu Q L, Zhang L Y, Cheng B, et al. S-scheme heterojunction photocatalyst. Chem, 2020, 6, 1543
[5] Chao Y G, Zhou P, Li N, et al. Ultrathin visible-light-driven Mo incorporating In_2O_3-$ZnIn_2Se_4$ Z-scheme nanosheet photocatalysts. Adv Mater, 2019, 31, 1807226
[6] Gu Y, Wu A P, Jiao Y Q, et al. Two-dimensional porous molybdenum phosphide/nitride heterojunction nanosheets for pH-universal hydrogen evolution reaction. Angew Chem Int Ed, 2021, 60, 6673
[7] Khan S, Je M, Ton N N T, et al. C-doped ZnS-ZnO/Rh nanosheets as multijunctioned photocatalysts for effective H_2 generation from pure water under solar simulating light. Appl Catal B, 2021, 297, 120473
[8] Ran L, Hou J G, Cao S Y, et al. Defect engineering of photocatalysts for solar energy conversion. Sol RRL, 2020, 4, 1900487
[9] Liu M, Chen Y, Su J, et al. Photocatalytic hydrogen production using twinned nanocrystals and an unanchored NiS_x co-catalyst. Nat Energy, 2016, 1, 16151
[10] Barawi M, Collado L, Gomez-Mendoza M, et al. Conjugated porous polymers: Ground-breaking materials for solar energy conversion. Adv Energy Mater, 2021, 11, 2101530
[11] Wang J G, Chen Y J, Zhou W, et al. Cubic quantum dot/hexagonal microsphere $ZnIn_2S_4$ heterophase junctions for exceptional visible-light-driven photocatalytic H_2 evolution. J Mater Chem A, 2017, 5, 8451
[12] Yu H B, Huang J H, Jiang L B, et al. Enhanced photocatalytic tetracycline degradation using N-CQDs/OV-BiOBr composites: Unraveling the complementary effects between N-CQDs and oxygen vacancy. Chem Eng J, 2020, 402, 126187
[13] Gao D D, Wu X H, Wang P, et al. Selenium-enriched amorphous $NiSe_{1+x}$ nanoclusters as a highly efficient cocatalyst for photocatalytic H_2 evolution. Chem Eng J, 2021, 408, 127230
[14] Bai S, Jiang J, Zhang Q, et al. Steering charge kinetics in photocatalysis: Intersection of materials syntheses, characterization techniques and theoretical simulations. Chem Soc Rev, 2015, 44, 2893
[15] Chen F Y, Wu Z Y, Adler Z, et al. Stability challenges of electrocatalytic oxygen evolution reaction: From mechanistic understanding to reactor design. Joule, 2021, 5, 1704
[16] Zhang S R, Nguyen L, Zhu Y, et al. *In-situ* studies of nanocatalysis. Acc Chem Res, 2013, 46, 1731
[17] Zaera F. *In-situ* and operando spectroscopies for the characterization of catalysts and of mechanisms of catalytic reactions. J Catal, 2021, 404, 900
[18] van der Wal L I, Turner S J, Zečević J. Developments and advances in *in situ* transmission electron microscopy for catalysis research. Catal Sci Technol, 2021, 11, 3634
[19] Knop-Gericke A, Kleimenov E, Hävecker M, et al. X-ray photoelectron spectroscopy for investigation of heterogeneous catalytic processes. Adv Catal, 2009, 52, 213
[20] Ahmed M H M, Temperton R H, O'Shea J N. An *in situ* exploration of subsurface defect migration to a liquid water-exposed rutile TiO_2(110) surface by XPS. Surf Interface Anal, 2021, 53, 1013
[21] Zhang P, Li Y K, Zhang Y S, et al. Photogenerated electron transfer process in heterojunctions: *in situ* irradiation XPS. Small Methods, 2020, 4, 2000214
[22] Bordiga S, Groppo E, Agostini G, et al. Reactivity of surface species in heterogeneous catalysts probed by *in situ* X-ray absorption techniques. Chem Rev, 2013, 113, 1736
[23] Zaera F. New advances in the use of infrared absorption spectroscopy for the characterization of heterogeneous catalytic reactions. Chem Soc Rev, 2014, 43, 7624
[24] Wachs I E, Roberts C A. Monitoring surface metal oxide catalytic active sites with Raman spectroscopy. Chem Soc Rev, 2010, 39, 5002
[25] Kim H, Kosuda K M, van Duyne R P, et al. Resonance Raman and surface- and tip-enhanced Raman spectroscopy methods to study solid catalysts and heterogeneous catalytic reactions. Chem Soc Rev, 2010, 39, 4820
[26] Bakker M G, Fowler B, Bowman M K, et al. Experimental methods in chemical engineering: Electron paramagnetic resonance spectroscopy-EPR/ESR. Can J Chem Eng, 2020, 98, 1668
[27] Wu J B, Shan H, Chen W L, et al. *In situ* environmental TEM in imaging gas and liquid phase chemical reactions for materials research. Adv Mater, 2016, 28, 9686
[28] Grogger W, Hofer F, Kothleitner G, et al. An introduction to high-resolution EELS in transmission electron microscopy. Top Catal, 2008, 50, 200
[29] Besenbacher F, Lauritsen J V, Wendt S. STM studies of model catalysts. Nano Today, 2007, 2, 30
[30] Preet A, Lin T E. A review: Scanning electrochemical microscopy (SECM) for visualizing the real-time local catalytic activity. Catalysts, 2021, 11, 594
[31] Zhuang G X, Chen Y W, Zhuang Z Y, et al. Oxygen vacancies in metal oxides: Recent progress towards advanced catalyst design. Sci China Mater, 2020, 63, 2089
[32] Feng H F, Xu Z F, Ren L, et al. Activating titania for efficient electrocatalysis by vacancy engineering. ACS Catal, 2018, 8, 4288
[33] Hou T T, Xiao Y, Cui P X, et al. Operando oxygen vacancies for enhanced activity and stability toward nitrogen photofixation. Adv Energy Mater, 2019, 9, 1902319
[34] Kolmakova N, Kolmakov A. Scanning electron microscopy for *in situ* monitoring of semiconductor–liquid interfacial processes: Electron assisted reduction of Ag ions from aqueous solution on the surface of TiO_2 rutile nanowire. J Phys Chem C, 2010, 114, 17233
[35] Möbus G, Saghi Z, Sayle D C, et al. Dynamics of polar surfaces on ceria nanoparticles observed *in situ* with single-atom resolution. Adv Funct Mater, 2011, 21, 1971
[36] Bugnet M, Overbury S H, Wu Z L, et al. Direct visualization and control of atomic mobility at {100} surfaces of ceria in the environmental transmission electron microscope. Nano Lett, 2017, 17, 7652
[37] Cavalca F, Laursen A B, Kardynal B E, et al. *In situ* transmission electron microscopy of light-induced photocatalytic reactions. Nanotechnology, 2012, 23, 075705
[38] Zhang L X, Miller B K, Crozier P A. Atomic level *in situ* observation of surface amorphization in anatase nanocrystals during light irradiation in water vapor. Nano Lett, 2013, 13, 679
[39] Lu Y, Yin W J, Peng K L, et al. Self-hydrogenated shell promoting photocatalytic H_2 evolution on anatase TiO_2. Nat Commun, 2018, 9, 2752
[40] Yu S H, Jiang Y H, Sun Y, et al. Real time imaging of photocatalytic active site formation during H_2 evolution by *in situ* TEM. Appl Catal B, 2021, 284, 119743
[41] Rycenga M, Cobley C M, Zeng J, et al. Controlling the synthesis and assembly of silver nanostructures for plasmonic applications. Chem Rev, 2011, 111, 3669
[42] Bamwenda G R, Tsubota S, Nakamura T, et al. Photoassisted hydrogen production from a water-ethanol solution: A comparison of activities of Au–TiO_2 and Pt–TiO_2. J Photochem Photobiol A, 1995, 89, 177
[43] Priebe J B, Karnahl M, Junge H, et al. Water reduction with visible light: Synergy between optical transitions and electron transfer in Au-TiO_2 catalysts visualized by in situ EPR spectroscopy. An-

gew Chem Int Ed, 2013, 52, 11420
[44] Yang K S, Lu Y R, Hsu Y Y, et al. Plasmon-induced visible-light photocatalytic activity of Au nanoparticle-decorated hollow mesoporous TiO_2: A view by X-ray spectroscopy. J Phys Chem C, 2018, 122, 6955
[45] Ekande O S, Kumar M. Review on polyaniline as reductive photocatalyst for the construction of the visible light active heterojunction for the generation of reactive oxygen species. J Environ Chem Eng, 2021, 9, 105725
[46] Yuan Y, Guo R T, Hong L F, et al. A review of metal oxide-based Z-scheme heterojunction photocatalysts: Actualities and developments. Mater Today Energy, 2021, 21, 100829
[47] Di T M, Xu Q L, Ho W, et al. Review on metal sulphide-based Z-scheme photocatalysts. ChemCatChem, 2019, 11, 1394
[48] Sai L M, Kong X Y. Type II hybrid structures of TiO_2 nanorods conjugated with CdS quantum dots: Assembly and optical properties. Appl Phys A, 2014, 114, 605
[49] Zhu Y Y, Liu Y F, Lv Y H, et al. Enhancement of photocatalytic activity for $BiPO_4$ via phase junction. J Mater Chem A, 2014, 2, 13041
[50] Xue J W, Bao J. Interfacial charge transfer of heterojunction photocatalysts: Characterization and calculation. Surf Interfaces, 2021, 25, 101265
[51] Yang H. A short review on heterojunction photocatalysts: Carrier transfer behavior and photocatalytic mechanisms. Mater Res Bull, 2021, 142, 111406
[52] Wang L B, Cheng B, Zhang L Y, et al. *In situ* irradiated XPS investigation on S-scheme TiO_2@$ZnIn_2S_4$ photocatalyst for efficient photocatalytic CO_2 reduction. Small, 2021, 17, 2103447
[53] Beck A, Huang X, Artiglia L, et al. The dynamics of overlayer formation on catalyst nanoparticles and strong metal-support interaction. Nat Commun, 2020, 11, 3220
[54] Vincent J L, Crozier P A. Atomic level fluxional behavior and activity of CeO_2-supported Pt catalysts for CO oxidation. Nat Commun, 2021, 12, 5789
[55] Simpson B H, Rodríguez-López J. Emerging techniques for the *in situ* analysis of reaction intermediates on photo-electrochemical interfaces. Anal Methods, 2015, 7, 7029
[56] Nosaka Y, Nosaka A Y. Generation and detection of reactive oxygen species in photocatalysis. Chem Rev, 2017, 117, 11302
[57] Liu J Y, Wei Z D, Shangguan W F. Defects engineering in photocatalytic water splitting materials. ChemCatChem, 2019, 11, 6177
[58] Connor P A, Dobson K D, McQuillan A J. Infrared spectroscopy of the TiO_2/aqueous solution interface. Langmuir, 1999, 15, 2402
[59] Haschke S, Mader M, Schlicht S, et al. Direct oxygen isotope effect identifies the rate-determining step of electrocatalytic OER at an oxidic surface. Nat Commun, 2018, 9, 4565
[60] Lin W Y, Frei H. Photochemical and FT-IR probing of the active site of hydrogen peroxide in Ti silicalite sieve. J Am Chem Soc, 2002, 124, 9292
[61] Rong X, Parolin J, Kolpak A M. A fundamental relationship between reaction mechanism and stability in metal oxide catalysts for oxygen evolution. ACS Catal, 2016, 6, 1153
[62] Zandi O, Hamann T W. Determination of photoelectrochemical water oxidation intermediates on haematite electrode surfaces using operando infrared spectroscopy. Nat Chem, 2016, 8, 778
[63] Zou Z, Ye J, Sayama K, et al. Direct splitting of water under visible light irradiation with an oxide semiconductor photocatalyst. Nature, 2001, 414, 625
[64] Guo S H, Li Y H, Tang S W, et al. Monitoring hydrogen evolution reaction intermediates of transition metal dichalcogenides via operando Raman spectroscopy. Adv Funct Mater, 2020, 30, 2003035
[65] Peng Y H, Geng M J, Yu J Q, et al. Vacancy-induced 2H@1T MoS_2 phase-incorporation on $ZnIn_2S_4$ for boosting photocatalytic hydrogen evolution. Appl Catal B, 2021, 298, 120570
[66] Ye L Q, Ma Z Y, Deng Y, et al. Robust and efficient photocatalytic hydrogen generation of ReS_2/CdS and mechanistic study by on-line mass spectrometry and *in situ* infrared spectroscopy. Appl Catal B, 2019, 257, 117897
[67] Wang X, Wang X, Huang J, et al. Interfacial chemical bond and internal electric field modulated Z-scheme Sv-$ZnIn_2S_4$/$MoSe_2$ photocatalyst for efficient hydrogen evolution. Nat Commun, 2021, 12, 4112
[68] Nakamura R, Nakato Y. Primary intermediates of oxygen photoevolution reaction on TiO_2 (Rutile) particles, revealed by *in situ* FTIR absorption and photoluminescence measurements. J Am Chem Soc, 2004, 126, 1290
[69] Zhang M, de Respinis M, Frei H. Time-resolved observations of water oxidation intermediates on a cobalt oxide nanoparticle catalyst. Nat Chem, 2014, 6, 362
[70] Ding Q, Liu Y, Chen T, et al. Unravelling the water oxidation mechanism on $NaTaO_3$-based photocatalysts. J Mater Chem A, 2020, 8, 6812
[71] Fresno F, Galdón S, Barawi M, et al. Selectivity in UV photocatalytic CO_2 conversion over bare and silver-decorated niobium-tantalum perovskites. Catal Today, 2021, 361, 85
[72] Halmann M. Photoelectrochemical reduction of aqueous carbon dioxide on p-type gallium phosphide in liquid junction solar cells. Nature, 1978, 275, 115
[73] Marszewski M, Cao S W, Yu J G, et al. Semiconductor-based photocatalytic CO_2 conversion. Mater Horiz, 2015, 2, 261
[74] Rao H, Schmidt L C, Bonin J, et al. Visible-light-driven methane formation from CO_2 with a molecular iron catalyst. Nature, 2017, 548, 74
[75] Schreier M, Héroguel F, Steier L, et al. Solar conversion of CO_2 to CO using Earth-abundant electrocatalysts prepared by atomic layer modification of CuO. Nat Energy, 2017, 2, 17087
[76] Wang Y, Shang X, Shen J, et al. Direct and indirect Z-scheme heterostructure-coupled photosystem enabling cooperation of CO_2 reduction and H_2O oxidation. Nat Commun, 2020, 11, 3043
[77] Kou Y, Nabetani Y, Dai M S, et al. Direct detection of key reaction intermediates in photochemical CO_2 reduction sensitized by a rhenium bipyridine complex. J Am Chem Soc, 2014, 136, 6021
[78] Liu L J, Li Y. Understanding the reaction mechanism of photocatalytic reduction of CO_2 with H_2O on TiO_2-based photocatalysts: A review. Aerosol Air Qual Res, 2014, 14, 453
[79] Liu L J, Zhao C Y, Miller J T, et al. Mechanistic study of CO_2 photoreduction with H_2O on Cu/TiO_2 nanocomposites by *in situ* X-ray absorption and infrared spectroscopies. J Phys Chem C, 2017, 121, 490
[80] Wu J, Li X D, Shi W, et al. Efficient visible-light-driven CO_2 reduction mediated by defect-engineered BiOBr atomic layers. Angew Chem Int Ed, 2018, 57, 8719
[81] Chen S, Wang H, Kang Z, et al. Oxygen vacancy associated single-electron transfer for photofixation of CO_2 to long-chain chemicals. Nat Commun, 2019, 10, 788
[82] Zhu J C, Shao W W, Li X D, et al. Asymmetric triple-atom sites confined in ternary oxide enabling selective CO_2 photothermal reduction to acetate. J Am Chem Soc, 2021, 143, 18233
[83] Ren X J, Gao M C, Zhang Y F, et al. Photocatalytic reduction of CO_2 on BiOX: Effect of halogen element type and surface oxygen vacancy mediated mechanism. Appl Catal B, 2020, 274, 119063
[84] MacKay B A, Fryzuk M D. Dinitrogen coordination chemistry: The biomimetic borderlands. ChemInform, 2004, 35, 703
[85] Shen H D, Yang M M, Hao L D, et al. Photocatalytic nitrogen reduction to ammonia: Insights into the role of defect engineering in

photocatalysts. Nano Res, 2021, 275, 115
[86] Guo J P, Chen P. Catalyst: NH_3 as an energy carrier. Chem, 2017, 3, 709
[87] Medford A J, Hatzell M C. Photon-driven nitrogen fixation: Current progress, thermodynamic considerations, and future outlook. ACS Catal, 2017, 7, 2624
[88] Hoffman B M, Lukoyanov D, Yang Z Y, et al. Mechanism of nitrogen fixation by nitrogenase: The next stage. Chem Rev, 2014, 114, 4041
[89] Jia H P, Quadrelli E A. Mechanistic aspects of dinitrogen cleavage and hydrogenation to produce ammonia in catalysis and organometallic chemistry: Relevance of metal hydride bonds and dihydrogen. Chem Soc Rev, 2014, 43, 547
[90] Yuzawa H, Mori T, Itoh H, et al. Reaction mechanism of ammonia decomposition to nitrogen and hydrogen over metal loaded titanium oxide photocatalyst. J Phys Chem C, 2012, 116, 4126
[91] Hirakawa H, Hashimoto M, Shiraishi Y, et al. Photocatalytic conversion of nitrogen to ammonia with water on surface oxygen vacancies of titanium dioxide. J Am Chem Soc, 2017, 139, 10929
[92] Li C C, Wang T, Zhao Z J, et al. Promoted fixation of molecular nitrogen with surface oxygen vacancies on plasmon-enhanced TiO_2 photoelectrodes. Angew Chem, 2018, 130, 5376
[93] Li H, Shang J, Ai Z H, et al. Efficient visible light nitrogen fixation with BiOBr nanosheets of oxygen vacancies on the exposed {001} facets. J Am Chem Soc, 2015, 137, 6393
[94] Li P S, Zhou Z A, Wang Q, et al. Visible-light-driven nitrogen fixation catalyzed by Bi_5O_7Br nanostructures: Enhanced performance by oxygen vacancies. J Am Chem Soc, 2020, 142, 12430
[95] Wang S Y, Hai X, Ding X, et al. Light-switchable oxygen vacancies in ultrafine Bi_5O_7Br nanotubes for boosting solar-driven nitrogen fixation in pure water. Adv Mater, 2017, 29, 1701774
[96] Yang J H, Guo Y Z, Jiang R B, et al. High-efficiency "working-in-tandem" nitrogen photofixation achieved by assembling plasmonic gold nanocrystals on ultrathin titania nanosheets. J Am Chem Soc, 2018, 140, 8497
[97] Rao F, Zhu G Q, Zhang W B, et al. *In-situ* generation of oxygen vacancies and metallic bismuth from $(BiO)_2CO_3$ via N_2-assisted thermal-treatment for efficient selective photocatalytic NO removal. Appl Catal B, 2021, 281, 119481
[98] Shang H, Li M Q, Li H, et al. Oxygen vacancies promoted the selective photocatalytic removal of NO with blue TiO_2 via simultaneous molecular oxygen activation and photogenerated hole annihilation. Environ Sci Technol, 2019, 53, 6444
[99] Jin H, You R, Zhou S, et al. *In-situ* DRIFTS and XANES identification of copper species in the ternary composite oxide catalysts CuMnCeO during CO preferential oxidation. Int J Hydrog Energy, 2015, 40, 3919
[100] Zigah D, Rodríguez-López J, Bard A J. Quantification of photoelectrogenerated hydroxyl radical on TiO_2 by surface interrogation scanning electrochemical microscopy. Phys Chem Chem Phys, 2012, 14, 12764
[101] Kreuzer L B, Patel C K. Nitric oxide air pollution: Detection by optoacoustic spectroscopy. Science, 1971, 173, 45
[102] Jin S, Dong G H, Luo J M, et al. Improved photocatalytic NO removal activity of $SrTiO_3$ by using $SrCO_3$ as a new co-catalyst. Appl Catal B, 2018, 227, 24
[103] Lu Y F, Huang Y, Zhang Y F, et al. Oxygen vacancy engineering of $Bi_2O_3/Bi_2O_2CO_3$ heterojunctions: Implications of the interfacial charge transfer, NO adsorption and removal. Appl Catal B, 2018, 231, 357
[104] Nakamura R, Imanishi A, Murakoshi K, et al. *In situ* FTIR studies of primary intermediates of photocatalytic reactions on nanocrystalline TiO_2 films in contact with aqueous solutions. J Am Chem Soc, 2003, 125, 7443

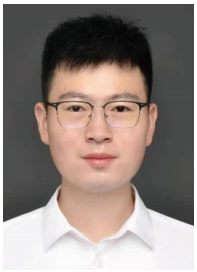

Zhen Fang received his MS from Wuhan University of Technology in 2021. Now he is a PhD candidate student at Shanghai Jiao Tong University under the supervision of Prof. Jianbo Wu. His research focuses on *in-situ* TEM characterization, and platinum-based electrocatalyst.

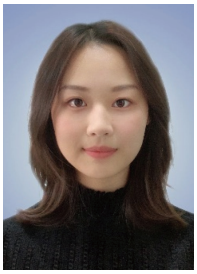

Yao Liu received her MS from Hunan University in 2021. Now she is a PhD candidate student at Shanghai Jiao Tong University under the supervision of Prof. Xiaoqin Zeng. Her research focuses on *in-situ* corrosion of metals and alloys.

Xiaoqin Zeng received his PhD degree from Shanghai Jiao Tong University in 2001, and now he is a professor in the School of Materials Science and Engineering at Shanghai Jiao Tong University. He was a recipient of the National Science Foundation for outstanding young scholars. His main research interests include strengthening theory and method of alloys and design and preparation of advanced Mg alloys.

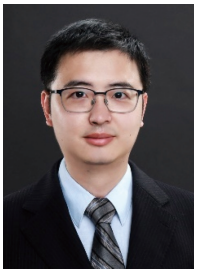

Jianbo Wu is a professor in the School of Materials Science and Engineering at Shanghai Jiao Tong University. He received his PhD degree in Chemical Engineering from University of Rochester in 2012, his MS degree in 2007 and BE degree in 2005 both in Materials Science and Engineering from Zhejiang University. He received postdoctoral training in the Department of Materials Science and Engineering at the University of Illinois at Urbana-Champaign. His current research focuses on facet and composition controlled nanocrystals, fuel cell electrocatalysts, functional materials for energy and environmental applications, and in situ TEM characterization.